OPEN

NPG Asia Materials (2014) 6, e103; doi:10.1038/am.2014.28

www.nature.com/am

ORIGINAL ARTICLE

Quantum dot and π-conjugated molecule hybrids: nanoscale luminescence and application to photoresponsive molecular electronics

Yoon Deok Han[1], Yong-baek Lee[1], Sungyeoun Park[2], Sumin Jeon[2], Arthur J Epstein[3], Ji-Hee Kim[4], Jeongyong Kim[4,5], Kwang-Sup Lee[2] and Jinsoo Joo[1]

Hybrid nanoparticles (NPs) consisting of an *n*-type CdSe/ZnS quantum dot (QD) as a core and *p*-type π-conjugate molecules as a shell were fabricated, and their nanoscale photoluminescence (PL) and photoresponsive molecular electronic characteristics were investigated. π-Conjugated macromolecular dioctyloxybenzodithiophene-based polythiophene (P3000) or a single carbazole (CB) molecule with insulating molecular blocks were attached to the QD surface. The nanoscale PL characteristics for the single QD were drastically changed through close contact with P3000 owing to energy and charge transfer effects. However, for the hybrid QD-CB NP, the PL of the QD was dominant because of weak energy transfer resulting from the relatively longer insulating molecular block between the QD and the CB molecule. From time-resolved PL spectra, the exciton lifetimes of the QD in the hybrid QD-P3000 and QD-CB NPs were clearly different because of a variation in the energy transfer rate. The photocurrents of the single hybrid QD-P3000 NP were considerably higher and actively responded to both forward and reverse biases due to the energy and charge transfer effects, while those of the single QD-CB NP exhibited diode characteristics. The QD-based hybrids show distinct nanoscale PL features and photoresponsive molecular electronic characteristics depending on the structures of π-conjugated molecules.
NPG Asia Materials (2014) **6,** e103; doi:10.1038/am.2014.28; published online 6 June 2014

Keywords: π-conjugate molecule; charge transfer; energy transfer; molecular electronics; photoluminescence; quantum dot

INTRODUCTION

Zero-dimensional semiconducting CdSe quantum dots (QDs) have unique optical properties, such as high quantum yield and emission spectra that are tunable by the quantum confinement effect.[1–4] The dark-state currents of the QDs obtained using colloidal CdSe, self-assembled InAs, GeSi and Ge have been measured in the range of 1–1000 pA by using a conducting atomic force microscopy (CAFM),[5–8] and their current–voltage (*I–V*) characteristic curves revealed typical semiconducting behavior with a charge tunneling mechanism.[5] Considerable effort directed at modifying the surface of QDs using capping agents has led to a simple solution-based process, the stabilization of QDs and their uniform dispersion in solvent.[9]

π-Conjugated molecules with semiconducting properties are proposed as novel functional groups for the QDs in this study. The hybridization of *p*-type π-conjugated molecules to the surface of *n*-type QDs can induce distinct luminescence and charge transport characteristics because of energy and/or charge transfer effects.[10,11] QDs and π-conjugated molecule hybrids with controlled luminescent properties can be used for new active materials for light-emitting diodes in flexible displays. In addition, hybrids with an enhanced charge transfer efficiency can be used for nanoscale photovoltaic devices. Single molecule-based electronics using QDs and π-conjugated molecule hybrids with molecular-scale *n–p* or *n*-insulating (*ins*)–*p* heterojunction structures are new promising building blocks for nanoscale electronics and quantum device concepts.[12,13]

The control of energy and/or charge transfer efficiencies between the *n*-type QD and *p*-type π-conjugated molecules is based on the degree of their spectral overlap and the distance between the two systems, which are important issues for their application to bulk-scale optoelectronic devices and nanoscale molecule-based electronics. Along these lines, we designed and synthesized hybrid nanoparticles (NPs) consisting of a green CdSe/ZnS QD as a core and a π-conjugated dioctyloxybenzodithiophene-based polythiophene (P3000) as a shell (denoted as QD-P3000, which has a directly contacted *p–n–p* heterojunction structure (abbreviated as *n–p*

[1]Department of Physics, Korea University, Seoul, Korea; [2]Department of Advanced Materials, Hannam University, Daejeon, Korea; [3]Department of Physics, The Ohio State University, Columbus, OH, USA; [4]Center for Integrated Nanostructure Physics (CINAP), Institute of Basic Science (IBS), Sungkyunkwan University, Suwon, Korea and [5]Department of Energy Science, Sungkyunkwan University, Suwon, Korea
Correspondence: Professor K-S Lee, Department of Advanced Materials, Hannam University, 461-6 Jeonmin-Dong, Yuseong-Gu, Daejeon 305-811, Korea.
E-mail: kslee@hnu.kr
or Professor J Joo, Department of Physics, Korea University, Seoul 136-713, Korea.
E-mail: jjoo@korea.ac.kr
Received 17 August 2013; revised 15 February 2014; accepted 21 February 2014

junction)). We also synthesized a red CdSe/ZnS QD modified with an insulating block and *p*-type carbazole (CB) molecules as a shell (denoted as QD-CB, which has an *p–ins–n-ins–p* heterojunction structure (abbreviated as *n–ins–p* junction)), as shown in Figure 1. The novel properties of hybrids consisting of QDs attached to π-conjugated organic molecules may open new scientific and application fields for molecular electronics and optoelectronics, including luminescent displays and energy harvesting cells.

In this study, the nanoscale photoluminescence (PL) and photoresponsive molecular electronic characteristics were investigated for hybrid QD/π-conjugated molecule NPs. The PL intensity of a single QD-P3000 NP decreased considerably due to energy and charge transfer effects between the QD and P3000. For a single *n-ins-p*-type QD-CB NP, the luminescence of the QD was dominant due to the presence of the long insulating molecule, which resulted in a relatively weak energy transfer between the QD and the CB molecule. The different energy transfer rates of the QD and π-conjugated hybrids were confirmed by the presence of variations in the QD exciton lifetimes determined using time-resolved PL decay curves and transient absorption (TA) characteristics. According to the photoresponsive molecular electronic characteristics examined through CAFM experiments, the photocurrents of a single QD-P3000 NP were relatively higher and symmetric for both forward and reverse bias because of energy and charge transfer effects. The photocurrents of the single QD-CB NP showed diode characteristics due to the molecular insulating block.

EXPERIMENTAL PROCEDURE

Sample preparation

CdSe (core) and ZnS (shell) QDs were prepared using a single-step synthetic method.[14] For the passivation of core CdSe QDs, which maintained their quantum characteristics, a wider band gap material such as ZnS or CdS was generally used for a shell.[15–17] As the CdSe QDs have a high electron mobility compared with *p*-type organic materials, it was assumed that the QDs are *n*-type.[18] To functionalize the surface of the green CdSe/ZnS core-shell QDs, *p*-type π-conjugated dioctyloxybenzodithiophene-based polythiophene

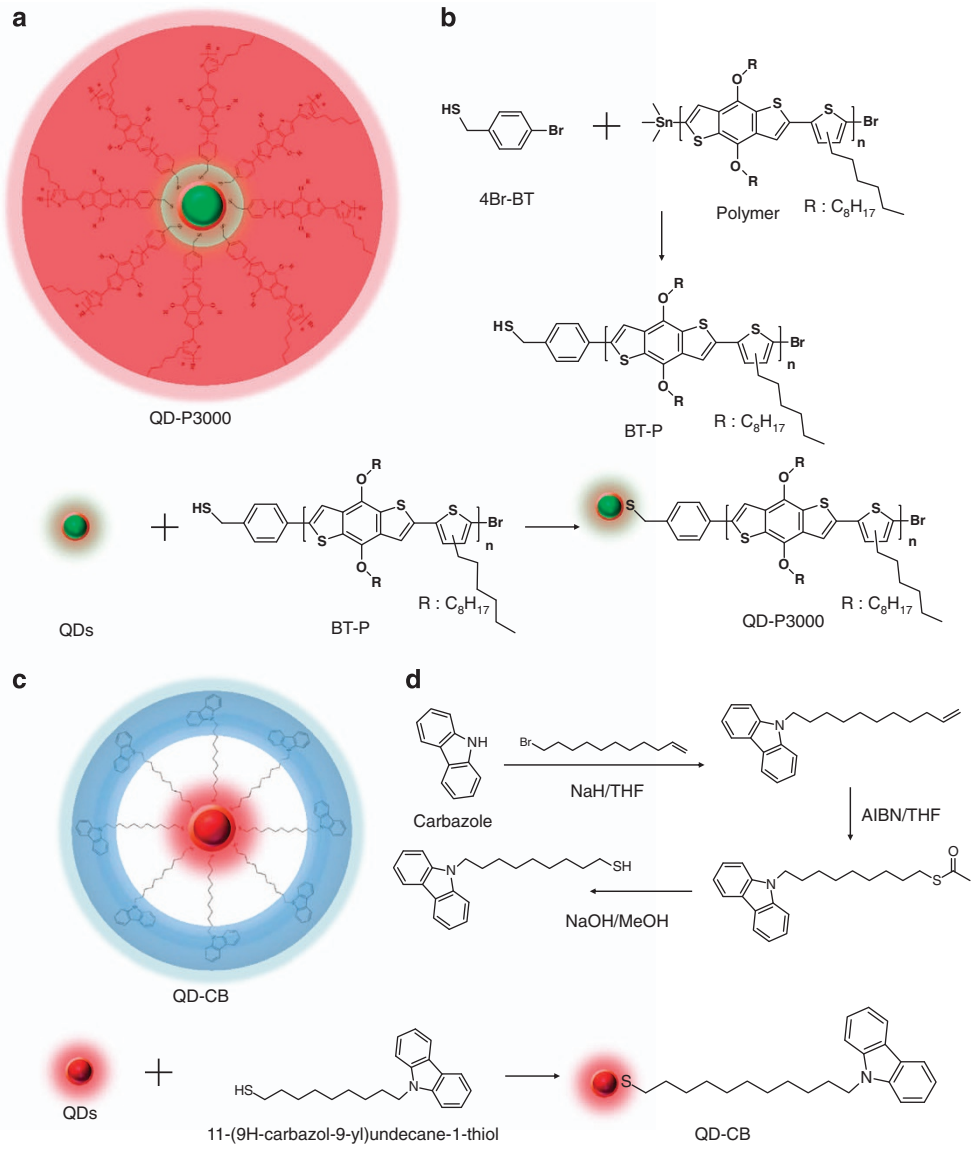

Figure 1 Schematic chemical structures of (**a**) QD-P3000 and (**c**) QD-CB hybrid NPs. Schematic synthetic procedures of (**b**) QD-P3000 and (**d**) QD-CB hybrid NPs.

(P3000) macromolecules were synthesized and hybridized, as shown in Figure 1a. The monomer for P3000 with a molecular weight of 3000 was prepared through the Stille coupling reaction.[19] We added 4Br-BT for polymerization and obtained benzodithiophene-based polythiophene (BT-P). For the ligand exchange on the surface of the QDs, QDs with BT-P and oleic acid (OA) attached in a 1:3 weight ratio were dispersed in dichlorobenzene and then sonicated. After sonication, the solution was centrifuged to remove residual ligands. Finally, the ligand of the QDs was exchanged from OA to BT-P. The schematic synthesis procedure of QD-P3000 is shown in Figure 1b. Note that the QD-P3000 hybrid NP has a directly contacted *n–p* heterojunction, which was designed for efficient energy/charge transfer.

As counterpart hybrid NPs, *n*-type red CdSe/ZnS QDs were hybridized with *p*-type CB molecules with an insulating undecane group, as shown in Figure 1c. A solution of CB 0.5 g (3 mmol) in tetrahydrofuran (THF) was combined with sodium hydride (NaH) 0.2 g (8 mmol) at room temperature. After stirring, the CB and NaH mixture was added dropwise to a solution of 11-bromo-1-undecene 0.7 ml in THF (3 ml) at 75 °C. The final mixture was stirred for 24 h at the same temperature. After quenching the reaction mixture by water and removing the THF solvent, the reaction mixture was extracted with methylene chloride (MC) and the organic layer was dried with $MgSO_4$ and concentrated. Purification by silica gel chromatography (only hexane) afforded the desired product 9-(undec-10-enyl)-9 H-CB. A solution of 9-(undec-10-enyl)-9 H-carbazole (0.57 g) in THF (30 ml) was combined with thioacetic acid (0.2 ml) and azobisisobutyronitrile (AIBN) (0.009 g) at room temperature. After stirring for 24 h at 60–70 °C, the reaction mixture was purified using silica gel chromatography (MC: Hexane = 1:1) to get the product S-11-(9H-carbazol-9-yl)undecyl ethanethioate. A solution of S-11-(9H-carbazol-9-yl)undecyl ethanethioate (1.0 mmol) in acetone (10 ml) was combined with 3 M sodium hydroxide (NaOH) 10 ml at room temperature. This reaction mixture was stirred for 1–2 h. After the reaction, the mixture was extracted with MC and 1 M hydrochloric acid (HCl) and dried by $MgSO_4$. Purification by silica gel chromatography (MC: hexane = 1:4) afforded the desired product 11-(9H-carbazol-9-yl)undecane-1-thiol. An illustration of the synthesis procedure of 11-(9H-carbazol-9-yl)undecane-1-thiol is shown in Figure 1d. Red CdSe/ZnS QDs with 11-(9H-carbazol-9-yl)undecane-1-thiol and OA attached were homogeneously dispersed in dichlorobenzene and then sonicated. After sonication, the solution was centrifuged to remove residual ligands. The ligand of the QDs was exchanged from OA to 11-(9H-carbazol-9-yl)undecane-1-thiol (Figure 1d).

When the binding affinity of a new ligand is stronger than that of the present ligand on the QD surface, the new ligand may replace the present ligand.[20–24] From the known ligand chemistry, thiol groups have the highest binding affinity to QD surfaces. One of the ends of P3000 and functionalized CB molecules have thiol groups that readily attach to the surface of QDs. For the QD-P3000 hybrid NP, π-conjugated P3000 macromolecules were directly attached to the surface of the QD for more efficient energy and/or charge transfer. However, for the QD-CB hybrid NP, insulating undecane molecules were placed between the QD and the CB molecules. The QD-P3000 and QD-CB hybrids are new molecule-based nanostructures with *n–p* and *n-ins–p* heterojunctions, respectively.

Measurements

The formation and surface morphologies of the QD-P3000 and QD-CB hybrid NPs were investigated using a field emission transmission electron microscope (FE-TEM, JEM-3010, JEOL) and electron energy loss spectroscopy (EELS, JEM-3010, JEOL). The ultraviolet and visible (UV–vis) absorption spectra of QD-P3000 and QD-CB NPs in dichlorobenzene solution were measured using an Agilent 8453 spectrometer (Santa Clara, CA, USA). The TA spectra of QD-P3000 and QD-CB NPs were measured using a Coherent Libra Series, TOPAS

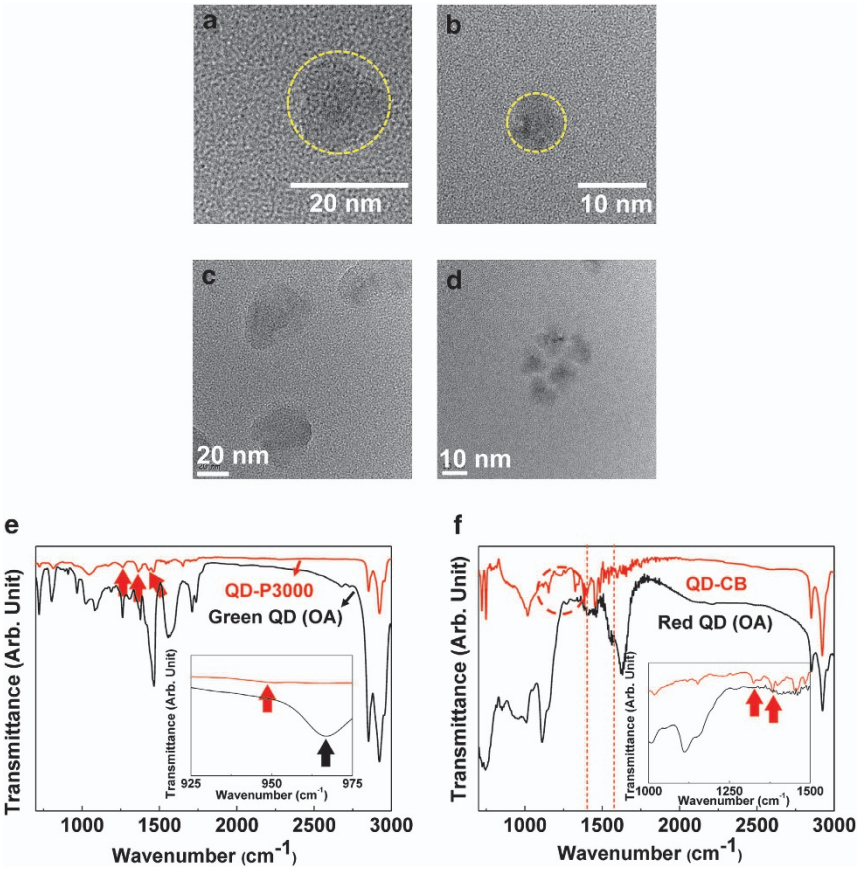

Figure 2 HR-TEM images of a single (**a**) QD-P3000 and (**b**) QD-CB hybrid NP. HR-TEM images of a few (**c**) QD-P3000 and (**d**) QD-CB hybrid NPs. FT-IR spectra of (**e**) OA-attached green QDs and QD-P3000 NPs and (**f**) OA-attached red QDs and QD-CB NPs. Insets: magnification of FT-IR spectra.

prime (Coherent, Santa Clara, CA, USA) as a light source and HELIOS TA spectrometer (Ultrafast Systems, Sarasota, FL, USA). The Fourier transform infrared (FT-IR) spectra of the samples were measured using an Infinity gold FT-IR Series (ThermoMattson, Waltham, MA, USA). For FT-IR measurements, the samples were homogeneously mixed with KBr and then dried. The solution PL spectra of the green and red QDs in dichlorobenzene solution were measured using HITACHI F-7000 fluorescence spectrophotometers (Tokyo, Japan). For nanoscale PL characteristics in the solid state, the QDs and hybrid NPs were drop-cast onto a glass cover slip and the laser confocal microscope (LCM) PL spectra of the single NPs were measured using a homemade LCM (Monochromator: Acton spectra Pro 300i, CCD: Acton PIXIS 100, scan stage: PSIA XE-120) with a high spatial resolution (about 200 nm). A laser with an excitation wavelength of 405 nm was used in the LCM PL measurement system. The excitation power and acquisition time for the LCM PL mapping images were fixed at 10 μW and 47.5 ms, respectively. The detailed methods for the LCM experiment have been reported previously.[25,26] For direct comparison of the luminescence color and brightness, color charge-coupled device images (AVT Marlin F-033C, $\lambda_{ex} = 435$ nm) were acquired. For photoresponsive molecular electronic characteristics, the *I–V* curves of a single QD-P3000 or QD-CBNP spin-coated onto indium tin oxide glass at 500 r.p.m. were measured using a CAFM (NanoFocus Albatross, Seoul, Korea), with and without incident light. Using AFM scanning, single NPs were selected for *I–V* measurements. An unpolarized Ar-ion laser ($\lambda_{ex} = 488$ nm) with a power of 110 nW was used for the excitation of the NPs.

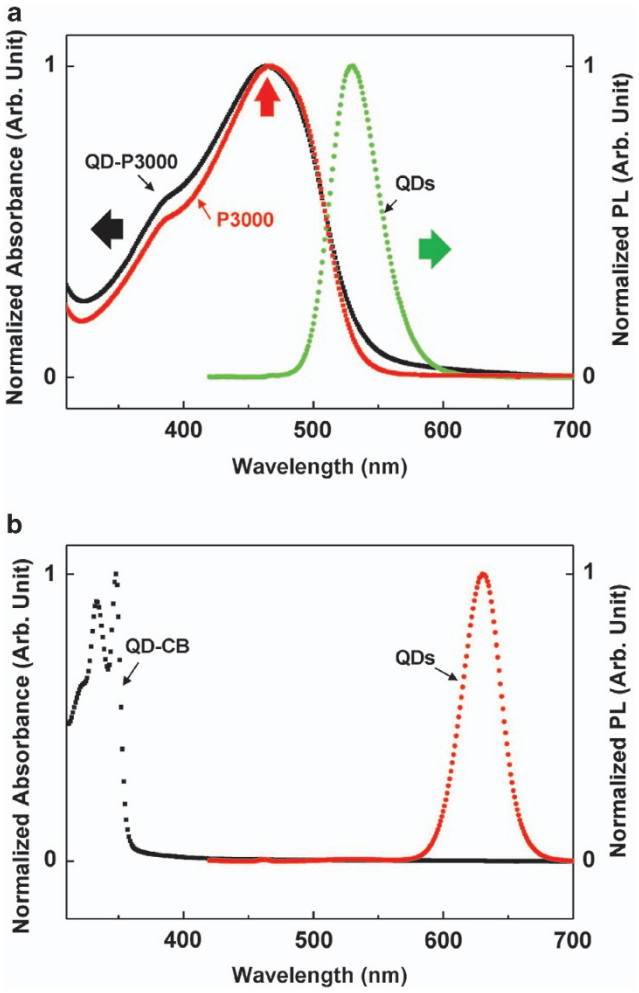

Figure 3 (**a**) Normalized UV–vis absorption spectrum of P3000 (red curve) and QD-P3000 (black curve) and solution PL spectrum (green curve) of green QDs. (**b**) Normalized UV–vis absorption spectrum (black curve) of QD-CB hybrid NPs and PL spectrum (red curve) of red QDs.

RESULTS AND DISCUSSION

Formation of QD and π-conjugated molecule hybrid NPs

Figures 2a and b show high-resolution transmission electron microscope (HR-TEM) images of single-hybrid QD-P3000 and QD-CB NPs. The diameters of QD-P3000 and QD-CB single NPs were estimated to be about 25 (±5) nm and 10 (±1) nm, respectively, which are close to the theoretical values obtained from the schematics in Figures 1a and b. Figures 2c and d show HR-TEM images of several hybrid QD-P3000 and QD-CB NPs, respectively, in which we observed a relatively similar size distribution of the NPs. Additional HR-TEM images and a histogram of the NP size distribution with several hundred particles are shown in Supplementary Figure S1. In the HR-TEM images, periodic striped patterns originating from the crystalline lattice of the QD were observed. The lattice constant of the inside of the CdSe QDs was estimated to be 3.4 Å, which agrees with previous results.[15] To confirm the hybrid structures, electron energy loss spectra were acquired. Oxygen from QD-P3000 and nitrogen from QD-CB were detected (see Supplementary Figure S2), indicating the attachment of the P3000 and CB groups to the QDs.

Figure 2e shows FT-IR spectra of the OA-attached green QDs and hybrid QD-P3000 NPs. The peaks at 2854 and 2925 cm^{-1} can be assigned to symmetric and anti-symmetric methylene stretching modes, respectively. The peaks at 1262, 1364 and 1458 cm^{-1}, due to C-C inter ring bond stretching, methyl deformation and symmetric ring stretching modes, respectively, were observed in QD-P3000 samples,[27–31] indicating the existence of P3000 macromolecules in the hybrid NPs. We also observed C-S stretching modes for the OA-attached green QDs and QD-P3000 NPs at 967 and 950 cm^{-1}, respectively (inset of Figure 2e). The shift in the C-S stretching mode also supports the hybridization of the QDs and P3000.[32,33] The FT-IR spectra of the hybrid QD-CB NPs and OA-attached red QDs are shown in Figure 2f. The peaks at 2854 and 2925 cm^{-1}, due to symmetric and anti-symmetric methylene stretching modes, respectively, were observed in QD-CB NPs and red QDs. The C-N stretching modes at 1324 and 1384 cm^{-1} that originated from CB molecules were observed for the QD-CB hybrid NPs, but not for the OA-attached red QDs, suggesting that the functionalized CB molecules were attached to the QD surface.[34]

Optical absorption and PL spectra in solution

Figure 3a shows the normalized UV–vis absorption spectra of the P3000 and QD-P3000 samples, as well as the solution PL spectrum of the constituent green QDs in a chloroform solution. The π-π* transition peak of P3000 was observed at about 460 nm with a shoulder peak at 390 nm. The absorption spectrum of the QD-P3000 was slightly broader than that of the P3000. The PL peak of the green QDs was observed at 530 nm, as shown in Figure 3a. The emission spectrum of the green QDs and the absorption spectrum of the hybrid QD-P3000 NPs partially overlapped by about 26.7% in terms of the spectral area. Therefore, it can be expected that energy transfer occurs from the *n*-type QDs to the *p*-type P3000 when these two systems are close enough. Figure 3b shows the normalized UV–vis absorption spectrum of the QD-CB samples, and the solution PL spectrum of the red QDs. The π-π* transition peak of the *p*-type-functionalized CB molecules was observed at about 359 nm, and the PL peak of the red QDs was observed at 640 nm (Figure 3b). The energy transfer from the QDs to the CB molecules is more difficult compared with that from the CB molecules to the QDs because of the degree of overlap between the two spectra (see Figure 3 and Supplementary Figure S3). For the QD-CB hybrid NP, there are insulating undecane molecules (of about 20 Å in length) between the QDs and CB molecules, the

presence of which considerably hinders energy transfer compared with the QD-P3000 hybrid NP. As shown in Figures 1a and b, the *p*-type π-conjugated P3000 molecules were more closely attached to the surface of the QDs than the functionalized CB molecules. All of the UV–vis absorption and solution PL spectra of the materials studied here are shown in Supplementary Figure S4.

Nanoscale luminescence characteristics

To investigate the nanoscale PL characteristics, high-resolution LCM PL spectra ($\lambda_{ex} = 405$ nm) were measured for green or red light-emitting CdSe/ZnS QDs and the single-hybrid QD-P3000 and QD-CB NPs. Figure 4a shows the LCM PL spectra of the hybrid QD-P3000 NPs, with the decomposed curves, and of the green QDs. A very sharp and tall LCM PL peak (maximum photon counts = 3417) for the green QDs was observed at 530 nm. However, a relatively broad and weak LCM PL spectrum (maximum photon counts = 86) was observed for the single QD-P3000 NP. The LCM PL spectrum of the QD-P3000 hybrid showed a main peak at 530 nm, with weak shoulder peaks at about 630 nm. The broad shoulder peaks originated from P3000 (see Supplementary Figure S5). The LCM PL intensity corresponding to the green QD ($\lambda_{max} = 530$ nm) in the hybrid QD-P3000 NP was drastically reduced because of the energy and charge transfer effects from the QD to P3000. The spectral overlap in Figure 4a and the decrease in exciton lifetime (discussed later) support energy and charge transfer effects. From the color charge-coupled device images of the green QDs and the hybrid QD-P3000 NPs shown in the insets of Figure 4a, we can directly confirm the drastic decrease of the brightness of the QDs after hybridization with P3000.

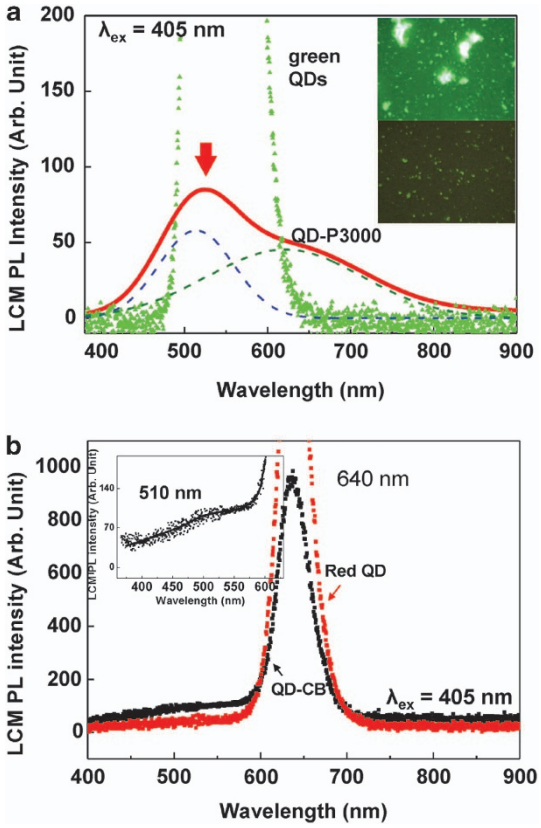

Figure 4 (**a**) LCM PL spectra of green QDs (green dots) and QD-P3000 single NPs (red curve). The dotted curves are the decomposed spectra for the QD-P3000 NP. Top and bottom insets: color charge-coupled device images of green QDs and QD-P3000 NPs, respectively. (**b**) LCM PL spectra of red QDs (red dots) and QD-CB single NPs (black dots). Insets: magnification of LCM PL spectrum of the QD-CB NPs in the wavelength range 360–630 nm.

Figure 4b shows the LCM PL spectrum of the single-hybrid QD-CB NPs. A relatively high LCM PL peak (maximum photon counts = 1805) at 640 nm was observed for the red QDs. The LCM PL peak of the red QD part of the hybrid QD-CB NP was observed at 640 nm, with a maximum photon count of 986. A relatively weak shoulder peak was also observed at about 510 nm because of the CB molecules, as shown in the inset of Figure 4b. For the hybrid QD-CB NP, dominance by the red QDs was observed in the LCM PL. The LCM PL intensity of the red QDs was not significantly reduced after hybridization with the functionalized CB molecules compared with the case of green QD after hybridization with P3000. The reduction ratios of maximum photon counts of the QD-P3000 and QD-CB NPs were estimated to be about 97.5% and 45.4%, respectively. These results suggest that energy and charge transfer was relatively weak in the QD-CB NPs because of both the lack of spectral overlap and the presence of insulating undecane molecules between the QD and CB molecules. Therefore, we can conclude that energy and charge transfer effects between the *n*-type QDs and the *p*-type π-conjugated molecules could be determined by the structure of the π-conjugated molecules and the intersystem distance.

Exciton dynamics

TA spectroscopy experiments were performed to investigate the charge transfer between *n*-type QDs and the *p*-type π-conjugated molecules. Figures 5a and b show TA spectra of QD-P3000 and QD-CB hybrid NPs, respectively, under the same experimental condition with the exception of excitation wavelength. The QD-P3000 and QD-CB hybrid NPs were excited by 510 and 620 nm laser pulse for the resonant excitation of QDs, respectively. In Figure 5a, which is the result of resonant excitation of the green QD, the strong negative signal was shown in QD-P3000 hybrid NPs at about 550 nm, implying the efficient charge transfer from the excited green QD to P3000. The green QD in the QD-P3000 hybrid NPs absorbed a 510-nm laser pulse and charge was transferred to the closely contacted P3000 macromolecule within a few picoseconds. The inset of Figure 5a shows the TA spectrum of each hybrid NP at 0.3 ps after laser pumping of 510 nm wavelength. We observed the negative bands from both samples, which correspond to the depletion of charge carriers responsible for the ground-state absorption of the hybrid structures or, alternatively, to the excitonic photobleaching. For QD-P3000, as shown in the inset of Figure 5a, the negative peak centered at 550 nm represents the ground-state absorption of QD; therefore, it is implied that QDs are well hybridized with conjugated molecules.[35] Note that QD-P3000 shows much stronger photobleaching behavior at ~550 nm than QD-CB at ~640 nm because of the closer contact between QD and P3000. We could also observe a relatively weak bleaching behavior for the QD-CB hybrid NPs at 640 nm, as shown in Figure 5b, due to inefficient charge transfer from the excited red QD to CB originating from the insulating molecular block. Charge transfer in the QD-CB hybrid NPs was much lower than that for the QD-P3000 hybrid NPs.

Time-resolved confocal PL (TrPL) experiments were performed to investigate the exciton lifetime (τ). Figures 6a and b show the TrPL decay curves of the hybrid QD-P3000 and QD-CB NPs, respectively, in comparison with the QDs alone. The τ_i and amplitude (A_i) of the *i*th exciton component were obtained from multi-exponential fitting

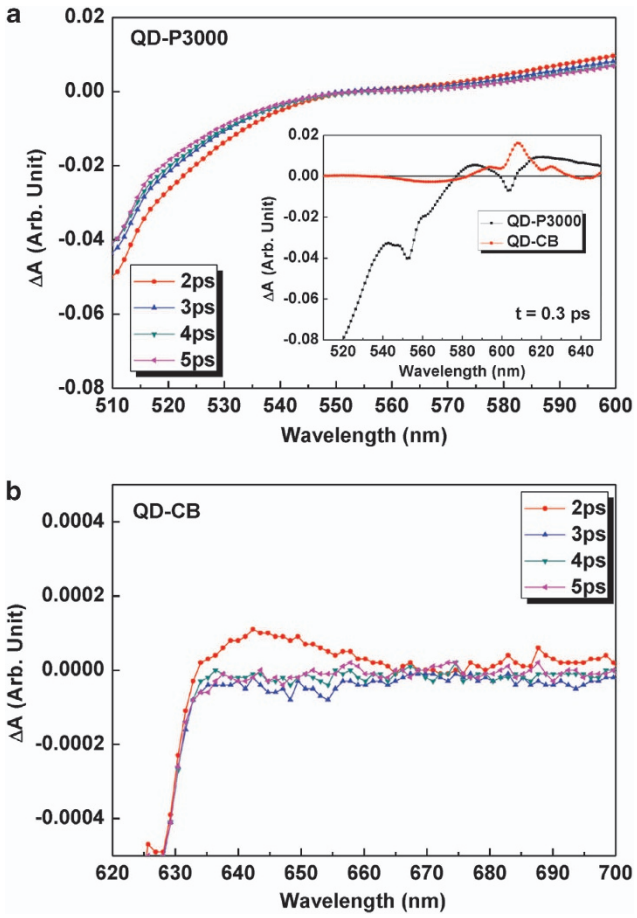

Figure 5 Transient absorption (time-resolved absorption difference) spectra of (**a**) QD-P3000 ($\lambda_{ex} = 510$ nm) and (**b**) QD-CB ($\lambda_{ex} = 620$ nm) hybrid NPs. Insets: time-resolved difference absorption spectra of corresponding hybrid NPs at 0.3 ps after laser pumping.

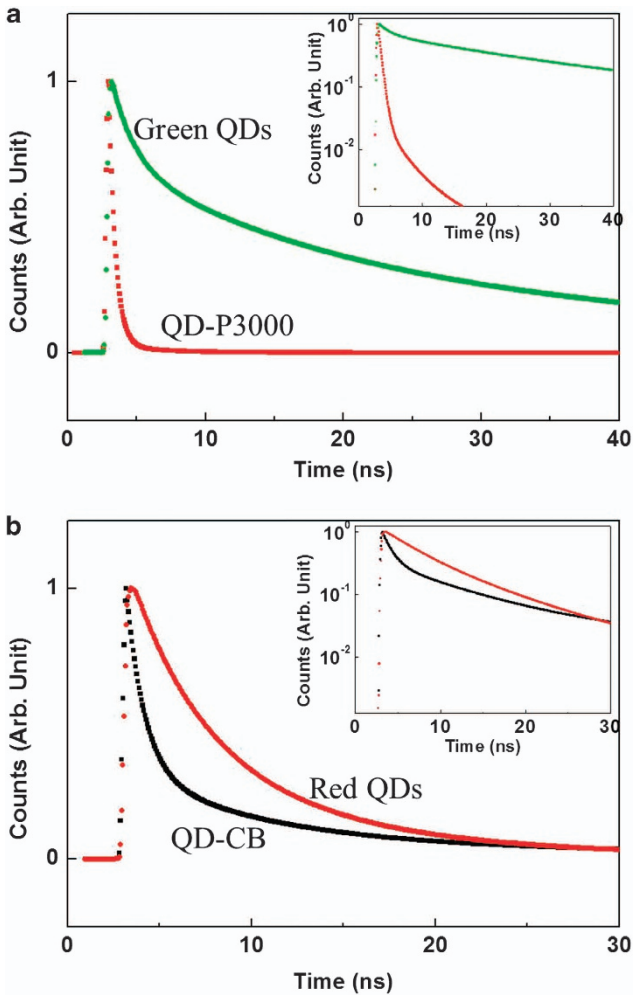

Figure 6 Normalized time-resolved PL decay curves of (**a**) green QDs and QD-P3000 NPs and of (**b**) red QDs and QD-CB NPs. Insets: normalized time-resolved PL decay curves for the corresponding samples on the logarithmic scale of the y-axis.

of the TrPL decay curves. The intensity-weighted average lifetime (τ_{avg}) was calculated from the equation $\tau_{avg} = \Sigma\ (A_i\tau_i^2/A_i\tau_i)$. Supplementary Table S1 lists τ_i, A_i and τ_{avg} values for the samples. The τ_{avg} values for the green QDs and QD-P3000 hybrids were estimated to be about 37.8 and 1.2 ns, respectively. τ_{avg} for the QD part of the hybrid QD-P3000 NPs was obtained from TrPL experiments using a bandpass filter at 530 nm. We observed a drastic decrease in τ_{avg} for the green QDs through hybridization with the *p*-type π-conjugated P3000. This decrease originated from the energy and charge transfer effects between the *n*-type QDs and *p*-type P3000. Assuming the total energy and charge transfer rate (E) is $E \equiv 1 - \tau_{DA}/\tau_D$, where τ_{DA} and τ_D are the exciton lifetimes of a donor with an acceptor and a donor without an acceptor, respectively, the *E*-value from the green QD to P3000 in the QD-P3000 hybrid NPs is calculated to be about 0.97.

Using a similar analogy, the τ_{avg} values of the red QDs and the hybrid QD-CB NPs were estimated to be 6.5 ns and 4.3 ns, respectively, from the results of Figure 6b. The value of τ_{avg} of the red QDs was not significantly changed through hybridization with the functionalized CB, suggesting a relatively weak energy and/or charge transfer effect. This weak effect originates from both the existence of a long insulating undecane molecular block and the weakness of the QD PL spectrum overlap with the optical absorption of the CB molecules. Therefore, the PL properties and τ_{avg} of the QD-CB NPs were dominated by the QD. The results of the exciton lifetimes from the TrPL experiments for the hybrid QD-P3000 and QD-CB NPs support the PL characteristics shown in Figure 4.

Photoresponsive molecular electronics

Figure 7a and its inset show an AFM surface profile and topographical image of a single QD-P3000 NP, respectively. The diameter of the QD-P3000 NP was estimated from the AFM surface profile to be about 25 nm, which agreed with the theoretical estimates for a QD diameter of ~7 nm and a P3000 length of ~2 × 7 nm. Figure 7b and its inset show an AFM surface profile and topographical image of the QD-CB, respectively. The total diameter of the QD-CB NP was estimated to be about 11 nm, which is close to the theoretical value (diameter of QD ~10 nm, length of functional CB ~2 nm). These single-hybrid NPs, consisting of the QD and π-conjugate molecules, were selected for measuring the photoresponsive *I–V* characteristics.

Figure 7c shows a schematic illustration of the photoresponsive *I–V* characteristic measurement for a single-QD-based hybrid NP using CAFM with incident light. A platinum-coated tip and ITO-coated glass were used as electrodes for the CAFM. Figures 7d and e show the

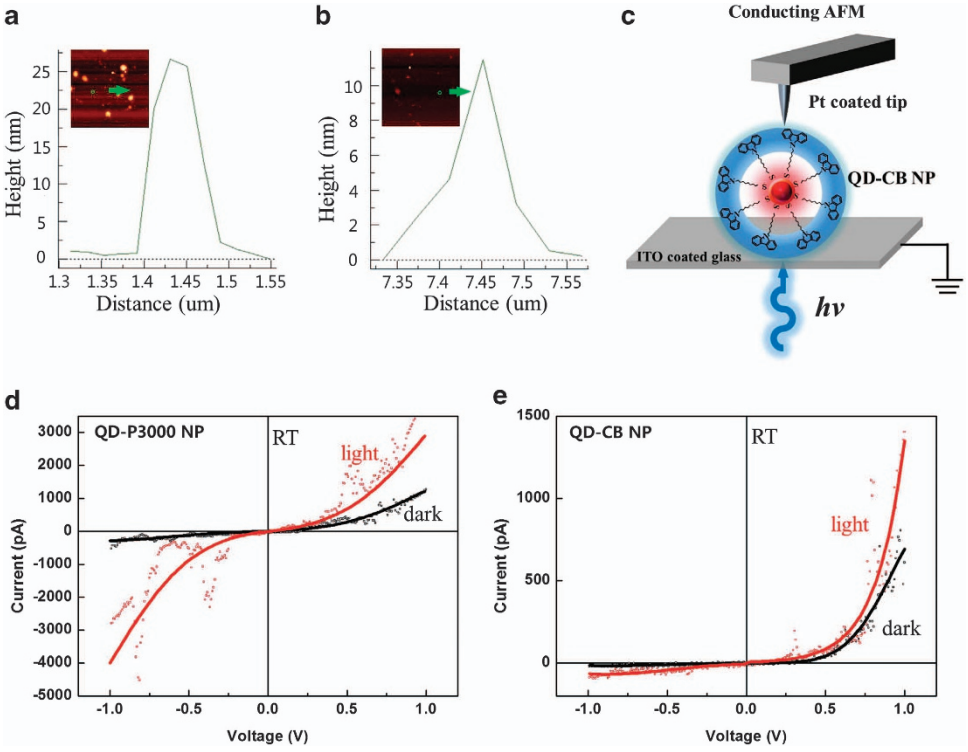

Figure 7 (**a**) AFM surface profile of a single QD-P3000 NP. Inset: AFM topographic image of the NPs on an ITO substrate. (**b**) AFM surface profile of a single QD-CB NP. Inset: AFM topographic image of the NPs on an ITO substrate. (**c**) Schematic illustration of the CAFM experiment for the photoresponsive *I–V* characteristics using a single QD-CB NP. (**d**) *I–V* characteristic curves of a single QD-P3000 NP in dark and light conditions at room temperature (RT). The solid curves were obtained from a best fit. (**e**) *I–V* characteristic curves of a single QD-CB NP in dark and light conditions. The solid curves were obtained from a best fit.

I–V characteristics of the single *n–p*-junction QD-P3000 and the *n-ins-p*-junction QD-CB NPs, respectively, under dark and light conditions. The solid curves in these figures were obtained from the best fitting of raw data (dotted markers). As shown in Figure 7d for the single *n–p*-junctioned QD-P3000 NP, the *I–V* characteristics in both dark and light states were relatively symmetric for the forward and reverse biases, and the current rapidly increased with light irradiation because of photo-induced charges. Compared with the *I–V* characteristics of a single green QD (see Supplementary Figure S7a), the current of the QD-P3000 NP was considerably higher, even though the distance between the electrodes was longer than that of the QD due to the presence of P3000. The results could be due to the charge transfer effect between the *n*-type QD and the *p*-type P3000, with easier charge injection and conduction through the *p*-type π-conjugated P3000 molecule. However, for the single *n-ins-p* junction QD-CB NP, the *I–V* characteristics were strongly asymmetric, exhibiting diode-like behavior, as shown in Figure 7e. Compared with the *I–V* characteristics of a single red QD (see Supplementary Figure S7b), the current of a single QD-CB NP was similar to that of a red QD, indicating that the majority of the current of the QD-CB NP was transported through the QD. The conductance (*G*) values of the QD-P3000 NPs in dark and light conditions were measured to be 183 and 551 Ω^{-1}, respectively, in the low bias region (the ohmic region at $|V| \leqslant 0.1$ V). However, the *G* values of the QD-CB NPs under dark and light conditions were about 10 and 112 Ω^{-1}, respectively. For other QD-P3000 and QD-CB NP samples, similar photoresponsive *I–V* characteristic curves were observed (see Supplementary Figure S8). Therefore, the photoresponsive *I–V* characteristics of the single hybrid NPs were reproducible.

In both dark and light states, the current levels of the QD-P3000 NP were higher than those of the QD-CB NP. For example, the photocurrent of the QD-P3000 was about 4400 pA at $V = +1$ V, while that of the QD-CB was about 1400 pA at $V = +1$ V. For the QD-P3000 NP, *p*-type P3000 molecules were closely attached to the *n*-type QD (see Figure 1), and charge transport in the P3000 macromolecule was much easier due to the rigid π-conjugated structure. The photo-induced charge transfer effect at the interface of the *n–p* heterojunction of the QD-P3000 NP could contribute to active electron and hole transport. However, for the QD-CB NP, the distance between the QD and CB molecules, due to the insulating undecane molecular blocks, was longer than 20 Å, which is a relatively long distance for efficient charge transfer.[36]

Photoresponsive molecular electronics, charge transport mechanism

To analyze the charge transport mechanism of the hybrid QD-P3000 and QD-CB NPs, the Fowler–Nordheim (F–N) tunneling model was used, as shown in Figure 8. The charge transport mechanism for semiconducting *n–p* junction structures can be explained in terms of the F–N tunneling model, $I \propto E^2 \exp(-\kappa/E)$, where *E* is the electric field strength and κ is a parameter that depends on the barrier shape and height.[37,38] F–N tunneling can be characterized by the quantum mechanical tunneling of charge through a triangular barrier created at the heterojunction boundary by applying a high electric field.[37,38] Figure 8a shows the dark and photoresponsive *I–V* characteristic curves of a single QD-P3000 NP in forward bias, based on the F–N tunneling model ($\ln(I/V^2)$ vs $1/V$ has a negative slope). The *I–V* characteristics of a single QD-P3000 NP were described by using the

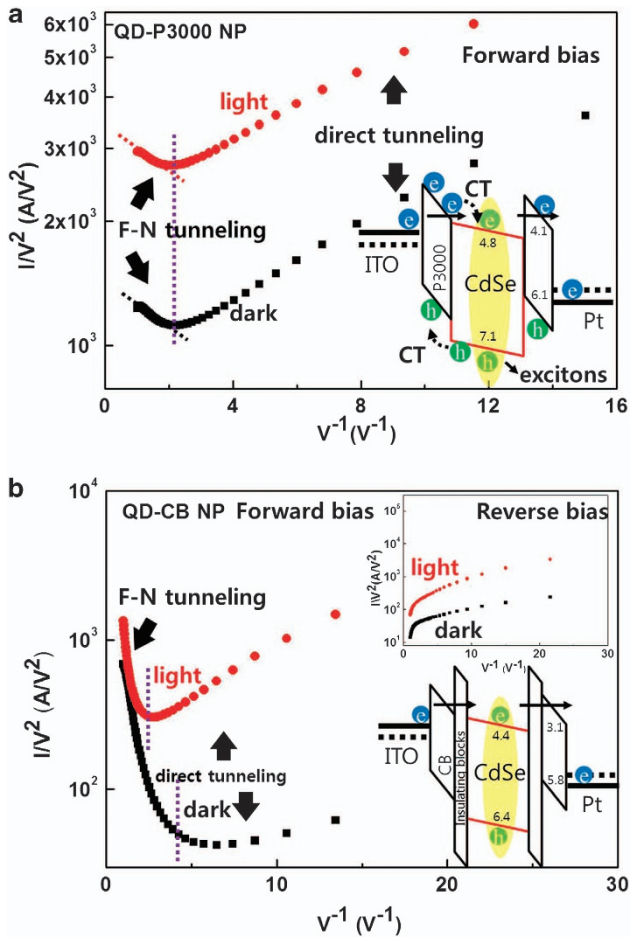

Figure 8 (**a**) *I–V* characteristic curves of a single QD-P3000 NP in dark and light conditions based on the Fowler–Nordheim (F–N) and direct tunneling models in forward bias. Inset: schematic energy band diagram for photoresponsive charge transport of the QD-P3000 under high forward bias. (**b**) *I–V* characteristic curves of QD-CB NP under dark and light conditions based on the F–N and direct tunneling models (in forward bias). Top inset: *I–V* characteristic curves for QD-CB NP under reverse bias. Bottom inset: schematic energy band diagram for photoresponsive charge transport of the QD-CB under high forward bias.

F–N tunneling model at high forward bias ($1/|V| \leqslant 2.0\,V^{-1}$), as shown in Figure 8a. The results imply charge tunneling through triangular barriers due to the P3000 material between the electrode and QD (or vice versa), as shown in the energy band diagram (inset of Figure 8a). However, the charge injection mechanism was described by direct tunneling in the low bias region ($1/|V| \geqslant 2.0\,V^{-1}$). Direct tunneling can be characterized by charge tunneling through a whole barrier (rather than a triangular shaped barrier) with a modest electric field.[37,38] In the low bias region, direct tunneling behavior ($\ln(I/V^2) \propto \ln(1/V)$ with a positive slope) was observed because the applied bias was too weak to overcome the barrier height. The observed transition from direct tunneling to F–N tunneling in Figure 8a has been reported for heterojunction structures such as metal–molecule–metal hybrid junctions or semiconducting organic–inorganic hybrid junctions.[39,40] In addition, the charge transport through the exterior P3000 only could be difficult because of non-coherent interchain interaction due to the disordered P3000 chains. The considerable enhancement of the current level of a single QD-P3000 NP through light irradiation is explained in terms of the additional contribution by the dissociation of photo-induced charges for the *n–p* heterojunction QD-P3000 hybrids, as shown in the energy band diagram (inset of Figure 8a). In reverse bias, the photoresponsive *I–V* characteristics of the QD-P3000 NP were similar to those in the forward bias (data not shown).

Figure 8b shows the *I–V* characteristic curves for a single QD-CB NP in dark and light conditions based on the F–N tunneling model. For forward bias, F–N tunneling (with negative slope) fit well to the charge transport mechanism in the high bias region ($1/|V| \leqslant 2.4\,V^{-1}$ in light conditions and $1/|V| \leqslant 4.6\,V^{-1}$ in dark conditions) due to the triangular potential barrier by applying high electric field. The charge transport mechanism changed to direct tunneling (with positive slope) in the low bias region. In the F–N tunneling regions, the *I–V* characteristics of single QD-CB and QD-P3000 NPs were different in that the photocurrent of the QD-CB was not significantly increased compared with the dark current ($1/|V| \leqslant 2.4\,V^{-1}$), as shown in Figure 8b. The CB molecules were not excited by the excitation laser ($\lambda_{ex} = 488$ nm). Therefore, the excitons in the QDs could only contribute to the photocurrent in the hybrid QD-CB NP. It is difficult to form photo-induced charge transfer excitons (or dissociated charges) because of the relatively long separation (~ 20 Å) between the QD and CB molecules. Therefore, the photocurrent was not significantly enhanced for the QD-CB NP. In the case of reverse bias, F–N tunneling behavior was not observed, and the charge transport mechanism of the QD-CB was described by direct tunneling in both dark and light conditions, as shown in the inset of Figure 8b, because of the high energy barrier between the Pt tip and the LUMO of the QD. It is difficult to transport the charges through the exterior functional CB groups because of a weak interchain interaction due to disorder.

We successfully modulated the nanoscale PL characteristics and photocurrent of *n*-type CdSe/ZnS QDs through the hybridization of *p*-type π-conjugated organic molecules with controlled intermolecular distance. The results obtained here were analyzed in terms of the energy and charge transfer effects based on the overlapping of optical spectra and the distance between donor and acceptor molecules. The energy and charge transfer effects were clearly observed for QD-P3000 due to the close contact of the *n*-type QD and *p*-type P3000. For the QD-CB hybrid NP, the energy and charge transfer effects were not effective due to the long insulating molecular blocks. Interesting further studies may be possible by using different types of QDs and π-conjugated organic molecules, with various intermolecular distances.

CONCLUSION

Core-shell-type *n–p* junction QD-P3000 and *n-ins-p* junction QD-CB hybrid NPs were fabricated, and their nanoscale PL and photoresponsive molecular electronic characteristics were investigated. For the QD-P3000 hybrid NPs, the LCM PL intensity from the green QD drastically decreased, and the photocurrent of the QD-P3000 was much higher and more symmetric compared with the QD-CB NP, suggesting more active energy and charge transfer between the *p*-type P3000 and the *n*-type QD due to the close contact of two nanosystems. However, for the QD-CB hybrid NPs, the red QD emission was dominant and the photocurrent showed a diode-like behavior because of the relatively weak energy transfer due to the existence of long insulating molecular blocks and the lack of spectral overlap. The nanoscale PL and molecular optoelectronic properties of hybrids consisting of QDs and π-conjugated molecules could be tuned by their relative distance and the degree of spectral overlap. We suggest that hybrid nanomaterials of *p*-type π-conjugated molecules

closely attached to *n*-type QDs, such as the QD-P3000 NP, can be used for nano- or molecular-scale photovoltaic units and active photoresponsive molecular devices. Hybrids consisting of QDs and π-conjugated molecules with controlled insulating molecular blocks can be used as active nanomaterials for displays and bio-sensors due to the simple method for tuning light emission color and as molecular rectifiers.

ACKNOWLEDGEMENTS

This work was supported by a National Research Foundation (NRF) grant funded by the Korean government (MEST) (No. 2012R1A2A2A01045102). K-S Lee acknowledges the funding for this work from the NRF through the Active Polymer Center for Patterned Integration (ERC R11-2007-050-01002-0). We also thank the Korea Basic Science Institute (KBSI) for the use of equipment for time-resolved PL confocal microscopy and HR-TEM.

1 Colvin, V. L., Schlamp, M. C. & Alivisatos, A. P. Light-emitting diodes made from cadmium selenide nanocrystals and a semiconducting polymer. *Nature* **370,** 354–357 (1994).
2 Norris, D. J., Efros, A. L., Rosen, M. & Bawendi, M. G. Size dependence of exciton fine structure in CdSe quantum dots. *Phys. Rev. B* **53,** 16347–16354 (1996).
3 Coe, S., Woo, W.-K., Bawendi, M. & Bulovic, V. Electroluminescence from single monolayers of nanocrystals in molecular organic devices. *Nature* **420,** 800–803 (2002).
4 Alivisatos, A. P. Semiconductor clusters, nanocrystals, and quantum dots. *Science* **271,** 933–937 (1996).
5 Tanaka, I., Kawasaki, E., Ohtsuki, O., Uno, K., Hara, M., Asami, H. & Kamiya, I. Conductive-tip atomic force microscopy of CdSe colloidal nanodots. *Surf. Sci* **532–535,** 801–805 (2003).
6 Tanaka, I., Kamiya, I., Sakaki, H., Qureshi, N., Allen, Jr S. J. & Petroff, P. M. Imaging and probing electronic properties of self-assembled InAs quantum dots by atomic force microscopy with conductive tip. *Appl. Phys. Lett.* **74,** 844–846 (1999).
7 Zhang, S. L., Xue, F., Wu, R., Cui, J., Jiang, Z. M. & Yang, X. J. Conductive atomic force microscopy studies on the transformation of GeSi quantum dots to quantum rings. *Nanotechnolgy* **20,** 135703 (2009).
8 Chung, H.-C., Chu, W.-H. & Liu, C.-P. Electron transport through individual Ge self-assembled quantum dots on Si. *Appl. Phys. Lett.* **89,** 082105 (2006).
9 William, W. Y., Emmanuel, C., Rebekah, D. & Vicki, L. C. Water-soluble quantum dots for biomedical applications. *Biochem. Bioph. Res. Co* **348,** 781–786 (2006).
10 Roth, P. J., Kim, K.-S., Bae, S. H., Sohn, B.-H., Theato, P. & Zentel, R. Hetero-telechelic dye-labeled polymer for nanoparticle decoration. *Macromol. Rapid Commun.* **30,** 1274–1278 (2009).
11 Zhao, L. & Lin, Z. Crafting semiconductor organic-inorganic nanocomposites via placing conjugated polymers in intimate contact with nanocrystals for hybrid solar cells. *Adv. Mater.* **24,** 4353–4368 (2012).
12 Akkerman, H. B., Blom, P. W. M., de Leeuw, D. M. & de Boer, B. Towards molecular electronics with large-area molecular junctions. *Nature* **441,** 69–72 (2006).
13 Aradhya, S. V. & Venkataraman, L. Single-molecule junctions beyond electronic transport. *Nat. Nanotechnol.* **8,** 399–410 (2013).
14 Bae, W. K., Char, K.-H., Hur, H. & Lee, S.-H. Single-step synthesis of quantum dots with chemical composition gradients. *Chem. Mater.* **20,** 531–539 (2008).
15 Dabbousi, B. O., Rodriguez-Viejo, J., Mikulec, F. V., Heine, J. R., Mattoussi, H., Ober, R., Jensen, K. F. & Bawendi, M. G. (CdSe)ZnS core-shell quantum dots: synthesis and characterization of a size series of highly luminescent nanocrystallites. *J. Phys. Chem.* **B101,** 9463–9475 (1997).
16 Hines, M. A. & Guyot-Sionnest, P. Synthesis and characterization of strongly luminescing ZnS-capped CdSe nanocrystals. *J. Phys. Chem.* **100,** 468–471 (1996).
17 Peng, X., Schlamp, M. C., Kadavanich, A. V. & Alivisatos, A. P. Epitaxial growth of highly luminescent CdSe/CdS core/shell nanocrystals with photostability and electronic accessibility. *J. Am. Chem. Soc.* **119,** 7019–7029 (1997).
18 Lee, J.-S., Kovalenko, M. V., Huang, J., Chung, D. S. & Talapin, D. V. Band-like transport, high electron mobility and high photoconductivity in all-inorganic nanocrystal arrays. *Nat. Nanotechnol.* **6,** 348–352 (2011).
19 Bao, Z., Chan, W. K. & Yu, L. Exploration of the Stille coupling reaction for the syntheses of functional polymers. *J. Am. Chem. Soc.* **117,** 12426–12435 (1995).
20 Dubois, F., Mahler, B., Dubertret, B., Doris, E. & Mioskowski, C. A versatile strategy for quantum dot ligand exchange. *J. Am. Chem. Soc.* **129,** 482–483 (2007).
21 Wuister, S. F., Donega, C. D. & Meijerink, A. J. Influence of thiol capping on the exciton luminescence and decay kinetics of CdTe and CdSe quantum dots. *J. Phys. Chem.* **B108,** 17393–17397 (2004).
22 Bullen, C. & Mulvaney, P. The effects of chemisorption on the luminescence of CdSe quantum dots. *Langmuir* **22,** 3007–3013 (2006).
23 Kalyuzhny, G. & Murray, R. W. Ligand effects on optical properties of CdSe nanocrystals. *J. Phys. Chem.* **B109,** 7012–7021 (2005).
24 Zhang, Q., Russell, T. O. & Emrick, T. Synthesis and characterization of CdSe Nanorods functionalized with regioregular poly(3-hexylthiophene). *Chem. Mater.* **19,** 3712–3716 (2007).
25 Hong, Y. K., Park, D. H., Park, S. K., Song, H., Kim, D.-C., Kim, J., Han, Y. H., Park, O. K., Lee, B. C. & Joo, J. Tuning and enhancing photoluminescence of light-emitting polymer nanotubes through electron-beam irradiation. *Adv. Funct. Mater.* **19,** 567–572 (2009).
26 Park, D. H., Kim, M. S. & Joo, J. Hybrid nanostructures using π-conjugated polymers and nanoscale metals: synthesis, characteristics, and optoelectronic applications. *Chem. Soc. Rev.* **39,** 2439–2452 (2010).
27 Kim, K., Shin, J. W., Lee, Y. B., Cho, M. Y., Lee, S. H., Park, D. H., Jang, D. K., Lee, C. J. & Joo, J. Poly(3-hexylthiophene)/multiwalled carbon hybrid coaxial nanotubes: nanoscale rectification and photovoltaic characteristics. *ACS Nano* **4,** 4197–4205 (2010).
28 Chen, T.-A., Wu, X. & Rieke, R. D. Regiocontrolled synthesis of poly(3-alkylthiophenes) mediated by Rieke zinc: their characterization and solid-state properties. *J. Am. Chem. Soc.* **117,** 233–244 (1995).
29 Kim, Y. H., Hotta, S. & Heeger, A. J. Photoexcitation and doping studies of poly(3-hexylthienylene). *Phys. Rev.* **B38,** 5490–5495 (1988).
30 Souto Maior, R. M., Hinkelmann, K., Eckert, H. & Wudl, F. Synthesis and characterization of two regiochemically defined poly(dialkylthiophenes): a comparative study. *Macromolecules* **23,** 1268–1279 (1990).
31 Hotta, S., Rughooputh, S. D. D. V., Heeger, A. J. & Wudl, F. Spectroscopic studies of soluble poly(3-alkylthienylenes). *Macromolecules* **20,** 212–215 (1987).
32 Young, A. G., Al-Salim, N., Green, D. P. & McQuillan, J. Attenuated total reflection infrared studies of oleate and trioctylphosphine oxide ligand adsorption and exchange reactions on CdS quantum dot films. *Langmuir* **24,** 3841–3849 (2008).
33 Koposov, A. Y., Cardolaccia, T., Albert, V., Badeava, E., Kilina, S., Meyer, T. J., Tretiak, S. & Sykora, M. Formation of assemblies comprising Ru-polypyridine complexes and CdSe nanocrystals studied by ATR-FTIR spectroscopy and DFT modeling. *Langmuir* **27,** 8377–8383 (2011).
34 Larrubia, M. A., Gutierrez-Alejandre, A., Ramirez, J. & Busca, G. A FT-IR study of the adsorption of indole, carbazole, benzothiophene, dibenzothiophene and 4,6-dibenzothiophene over solid adsorbents and catalysts. *Appl. Catal. A-Gen.* **224,** 167–178 (2002).
35 Medintz, I. L., Pons, T., Trammell, S. A., Grimes, A. F., English, D. S., Blanco-Canosa, J. B., Dawson, P. E. & Mattoussi, H. Interactions between redox complexes and semiconductor quantum dots coupled via a peptide bridge. *J. Am. Chem. Soc.* **130,** 16745–16756 (2008).
36 Forster, R. *Organic Charge-Transfer Complexes* (Academic Press, Waltham, MA, USA, 1969).
37 Sze, S. M. & Ng, K. K. *Physics of Semiconductor Devices*. 3rd edn (Wiley-Interscience, New York, 2007).
38 Parker, I. D. Carrier tunneling and device characteristics in polymer light-emitting diodes. *J. Appl. Phys.* **75,** 1656–1666 (1994).
39 Kergueris, C., Bourgoin, J.-P., Palacin, S., Esteve, D., Urbina, C., Magoga, M. & Joachim, C. Electron transport through a metal-molecule-metal junction. *Phys. Rev.* **B59,** 12505–12513 (1999).
40 Kagan, C. R. & Ratner, M. A. Molecular transport junction: an introduction. *MRS Bull.* **29,** 376–384 (2004).

Supplementary Information accompanies the paper on the NPG Asia Materials website (http://www.nature.com/am)